iScience

Article

Increased pathogenicity and transmissibility in hamsters of all age groups reveal an underestimated perniciousness of severe acute respiratory syndrome coronavirus 2 EG.1 variant

Graphical abstract

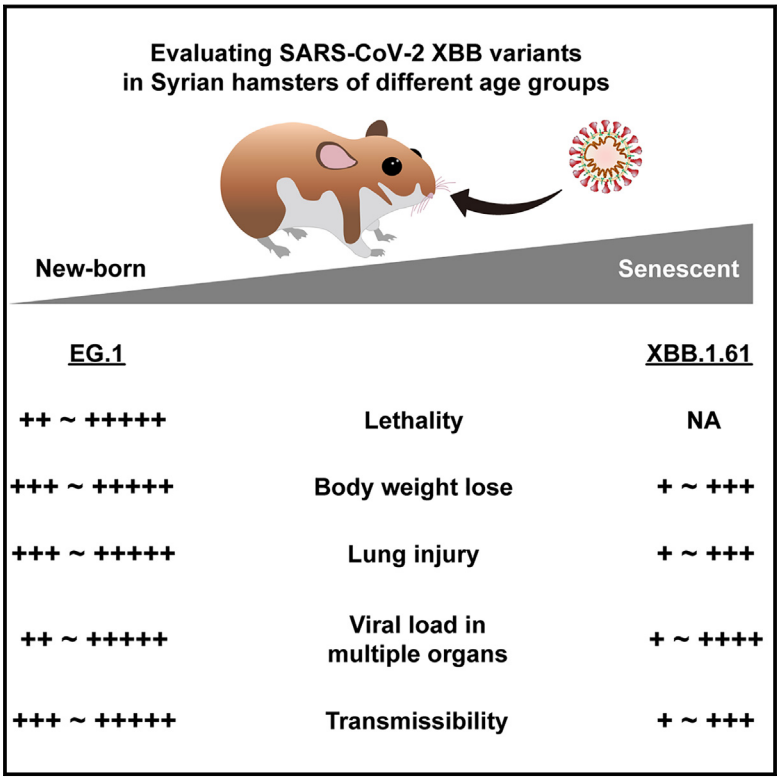

Highlights

- EG.1 shows increased pathogenicity and transmissibility over XBB.1.16 in hamsters
- EG.1 evolves to gain Q613H mutation on spike which is rarely detected in other XBB variants
- There is an underestimated perniciousness of EG.1 in all age groups of hamsters

Authors

Ming Zhou, Jian Ma, Mujin Fang, ..., Tong Cheng, Lunzhi Yuan, Ningshao Xia

Correspondence

tcheng@xmu.edu.cn (T.C.), yuanlunzhi@xmu.edu.cn (L.Y.), nsxia@xmu.edu.cn (N.X.)

In brief

Natural sciences; Biological sciences; Immunology; Immune response

Zhou et al., 2025, iScience *28*, 111875
March 21, 2025
https://doi.org/10.1016/j.isci.2025.111875

CellPress

iScience

CellPress
OPEN ACCESS

Article

Increased pathogenicity and transmissibility in hamsters of all age groups reveal an underestimated perniciousness of severe acute respiratory syndrome coronavirus 2 EG.1 variant

Ming Zhou,[1,5] Jian Ma,[1,5] Mujin Fang,[1,5] Xuan Liu,[2,5] Chang Zhang,[2] Kun Wu,[1] Jianghui Ye,[1] Yali Zhang,[1] Quan Yuan,[1,5] Rirong Chen,[3,4] Peiwen Chen,[3,4] Huachen Zhu,[3,4] Yi Guan,[3,4] Tong Cheng,[1,5,*] Lunzhi Yuan,[1,*] and Ningshao Xia[1,5,6,*]

[1]State Key Laboratory of Vaccines for Infectious Diseases, National Institute of Diagnostics and Vaccine Development in Infectious Diseases, School of Life Sciences, School of Public Health, Xiang an Biomedicine Laboratory, Xiamen University, Xiamen, Fujian, China

[2]Clinical Center for Bio-Therapy, Zhongshan Hospital, Fudan University (Xiamen Branch), Xiamen, Fujian, China

[3]State Key Laboratory of Emerging Infectious Diseases, School of Public Health, Li Ka Shing Faculty of Medicine, The University of Hong Kong, Hong Kong SAR, China

[4]Guangdong-Hong Kong Joint Laboratory of Emerging Infectious Diseases/Joint Laboratory for International Collaboration in Virology and Emerging Infectious Diseases, Joint Institute of Virology (STU/HKU), Shantou University, Shantou, Guangdong, China

[5]These authors contributed equally

[6]Lead contact

*Correspondence: tcheng@xmu.edu.cn (T.C.), yuanlunzhi@xmu.edu.cn (L.Y.), nsxia@xmu.edu.cn (N.X.)

https://doi.org/10.1016/j.isci.2025.111875

SUMMARY

The evolution and mutation of SARS-CoV-2 is elusive. However, the diverse *in vivo* pathogenicity and transmissibility of different SARS-CoV-2 Omicron/XBB variants are not well understood. We compared virological attributes of two XBB variants, XBB.1.16 and XBB.1.9.2.1 (EG.1) in new-born, juvenile, adult, middle-aged and senescent Syrian hamsters. In particular, EG.1 has a specific Q613H mutation and causes fatal severe pneumonia in hamsters of all ages. In contrast, all hamsters infected with XBB.1.16 survived and showed milder symptoms. The XBB.1.16 infected hamsters lost significantly less body weight and exhibited lower respiratory viral loads, pro-inflammatory cytokines and lung injury than those with EG.1 infection. In addition, EG.1 is more transmissible than XBB.1.16 in close contact co-housing. Both EG.1 and XBB.1.16 are highly resistant to therapeutic antibodies and convalescent serum. Overall, the unpredictable evolution, global transmission and potential threat of emerging SARS-CoV-2 variants necessitate the updating of prophylactic and therapeutic countermeasures in all age groups.

INTRODUCTION

Since the emergence of the severe acute respiratory syndrome coronavirus 2 (SARS-CoV-2) Omicron BA.1 variant in November 2021, the waves of subsequent Omicron and XBB variants spread worldwide from January 2022 to April 2024. Several dominant circulating variants including Omicron BA.1/BA.2, BA.5, BQ.1, XBB.1, XBB.1.5, XBB.1.16, XBB.1.9, EG.5.1, HK.3, BA.2.86/JN.1 and their progeny have accounted for the vast majority of the shares of reported cases. Important mutations in the spike protein and other regions of these emerging variants resulted in significant changes in their virological characteristics including pathogenicity, transmissibility, and ability to evade the immune system.

For example, the BA.1/BA.2 variant has many spike mutations such as G339D, R346K, S371L, S373P, S375F, K417N, N440K, G446S, S477N, T478K, E484A, Q493R, G496S, Q498R, N501Y, and Y505H, which significantly alter its tissue tropism, susceptibility, immune evasion capacity, pathogenicity and transmissibility in human respiratory epithelial cells and sensitive rodent models including the K18-hACE2 transgenic mouse and Syrian hamsters.[1–4] In contrast to the prototype virus and previous variants, the BA.1/BA.2 variant showed enhanced transmissibility, attenuated fusogenicity, viral replication, and tissue injury in the lungs of mice and hamsters. However, the subsequent dominant circulating BA.5 variant retains the L452R and F486V mutations, which is associated with viral fitness superior to BA.1/BA.2.[5] The pathogenicity of BQ.1.1 in hamsters is lower than that of BA.5, contributed by the additional mutations of R346T, K444T, N460K on the spike protein, as well as non-spike mutations including Q376K (NSP2), L260F (NSP6), Y273H (NSP12), M233I (NSP13), N268S (NSP13) and E136D (N).[6] Compared to BA.1/BA.2, the XBB/XBB.1 variant generally showed similar pathogenicity, but the additional mutations including V83A, Y144del, H146Q, Q183E, R346T, L368I, V445P, G446S, and F490Q,[7] increased their ability to

evade the antibodies induced by the vaccination or previous infections.

Following the SARS-CoV-2 pandemic, a high incidence of breakthrough infection has been reported in human populations worldwide. Host factors such as previous infection, vaccination, sex, and age may influence the outcome of SARS-CoV-2 infection. Previously, we reported the increased infectivity and pathogenicity of BA.1 in juvenile and senescent Syrian hamsters, suggesting that even a low-pathogenic SARS-CoV-2 variant may pose significant risks in specific human populations.[8] It is therefore necessary to evaluate the virological characteristics of emerging SARS-CoV-2 variants in sensitive animal models.

The vast majority of Omicron and XBB variants showed reduced pathogenicity, increased transmissibility, and increased ability to evade the immune system compared to the prototype virus and earlier Alpha, Beta, and Delta variants.[2,3,5–7,9] However, the unusual mutations and potential threats of a few emerging variants were not fully understood. Here we report the unique mutations and virological characteristics of the XBB.1.9.2.1 (EG.1) variant, which serves as the progeny virus of XBB.1.9 and the ancestral virus of EG.5.1. In contrast to a parallel prevalent variant, XBB.1.16, EG.1 showed several different mutations and a significant increase in pathogenicity and transmissibility in new-born, juvenile, adult, middle-aged and senescent Syrian hamsters.

RESULTS

Evolution and mutation patterns of the main variants of the severe acute respiratory syndrome coronavirus 2 omicron sublineage

To escape the herd immunity induced by infection and vaccination, SARS-CoV-2 evolves overtime. The phylogenetic tree inference and lineage monitoring for the dominant circulating SARS-CoV-2 variants were shown (Figures 1 and S1). The emergence of Omicron BA.1 variant initiated a new wave of pandemic in 2022 (Figure 1A). Afterward, BA.2 and BA.5 were reported as the main global circulating variants for several months. XBB variants replaced the dominant portion Omicron variants in early 2023 and have been continuously evolving. Several different XBB variants such as the XBB.1.5, XBB.1.16, XBB.1.9 family (include EG.1) and their progeny virus EG.5.1 spread worldwide. Recently, BA.2.86 and JN.1 is the main reported becoming the main circulating strains. In contrast of a previous circulating variant BA.1.16, EG.1 lost amino acid mutations include D1746Y, T19I, V83A, E180V, and T478R, and gain new mutations include T4175I, E484A and Q613H (Figure 1B). The progeny variant of EG.1, namely EG.5.1, gain mutations include A690V, A3143V, T19I, V83A, and F456L, and lost Q613H (Figure 1B). Notably, EG.1 has a different mutation pattern than most XBB variants, which implies significant changes in virological characteristics.

Disease outcome of severe acute respiratory syndrome coronavirus 2 EG.1 and XBB.1.16 infections in different age groups of hamsters

We first investigated the physiology and pathology changes after the infections of SARS-CoV-2 EG.1 and XBB.1.16 variants in hamsters in different age groups. The new-born (male and female, ~1 week), juvenile (male, 4–5 weeks), adult (male, 10–12 weeks), middle-aged (male, ~40 weeks), and senescent (male, ~80 weeks) hamsters were inoculated with 1×10^5 PFU of EG.1 or XBB.1.16 by nasal route, respectively. The new-born hamsters received an inoculation volume of 50 μL and the other age group received an inoculation volume of 200 μL. For each group, 12 hamsters were employed for evaluation. Survival rates were recorded from 0 to 7 days post infection (dpi). After the inoculation of EG.1, all of the 12 new-born hamsters deceased within five days, 7 out of the 12 senescent hamsters deceased within seven days, the juvenile, adult and middle-aged hamsters showed 60–80% survival rates, respectively (Figure 2A). Whereas, XBB1.16 infection is non-lethal in all of the five age groups (Figure 2B). Body weight changes of the survival hamsters were detected from 0 to 7 dpi. The new-born and senescent hamsters with EG.11 infection showed more than 20% of body weight loss at 5 and 7 dpi (Figure 2C). The adult and middle-aged hamsters exhibited 14.1 ± 3.6% and 17.2 ± 1.5% of body weight loss at 7 dpi of EG.1 infection (Figure 1C), suggesting a critical disease outcome. The body weight of EG.1-infected juvenile hamsters decreased from 0 to 5 dpi and slowly increased from 5 to 7 dpi (Figure 2C), implying a delay of body development. After the inoculation of XBB.1.16, the new-born and juvenile hamsters showed 5.8 ± 1.8% and 12.7 ± 1.1% of body weight increase, the adult, middle-aged and senescent hamsters showed 5.9 ± 1.3%, 9.8 ± 1.3% and 12.2 ± 1.4% of body weight loss from 0 to 7 dpi, respectively (Figure 2D).

To evaluate pulmonary pathology changes, lung lobes of the new-born hamsters deceased at 5 dpi, as well as the juvenile, adult, middle-aged and senescent hamsters euthanized at 7 dpi were collected and fixed for Hematoxylin & Eosin (H&E) staining. Notably, diffuse tissue apoptosis/necrosis, inflammatory immune cell infiltration, hemorrhage and mucous plug were observed in the lung lobes collected from the new-born, adult, middle-aged and senescent hamsters with EG.1 infection, as well as the middle-aged and senescent hamsters with XBB.1.16 infection (Figures 2E, S2, and S3). The juvenile hamsters with EG.1 infection, as well as the new-born, juvenile and adult hamsters with XBB.1.16 infection showed minimum to moderate lung injury (Figures 2E, S2, and S3). In addition, a comprehensive pathological scores were used to evaluate the severity of lung injury. The new-born, adult, juvenile, middle-aged and senescent hamsters with EG.1 infection showed 10.9 ± 0.9, 6.6 ± 2.5, 10.6 ± 1.7, 11.4 ± 0.9 and 11.9 ± 0.3 (Figure 1F; Table S1), however, those infected with XBB.1.16 showed 6.6 ± 2.7, 3.5 ± 1.8, 5.9 ± 1.7, 8.6 ± 2.3 and 10.5 ± 0.9 of lung comprehensive pathological scores, respectively (Figures 1F; Table S2). In conclusion, both XBB variants are highly pathogenic in middle-aged and senescent hamsters. Infection with EG.1 resulted in a worse disease prognosis than XBB.1.16 in all age groups of the hamster model.

Viral load in multiple organs of the hamsters infected with severe acute respiratory syndrome coronavirus 2 EG.1 and XBB.1.16 infections

We then analyzed viral RNA levels in respiratory organs, including the nasal turbinate, trachea, and lungs, and in major

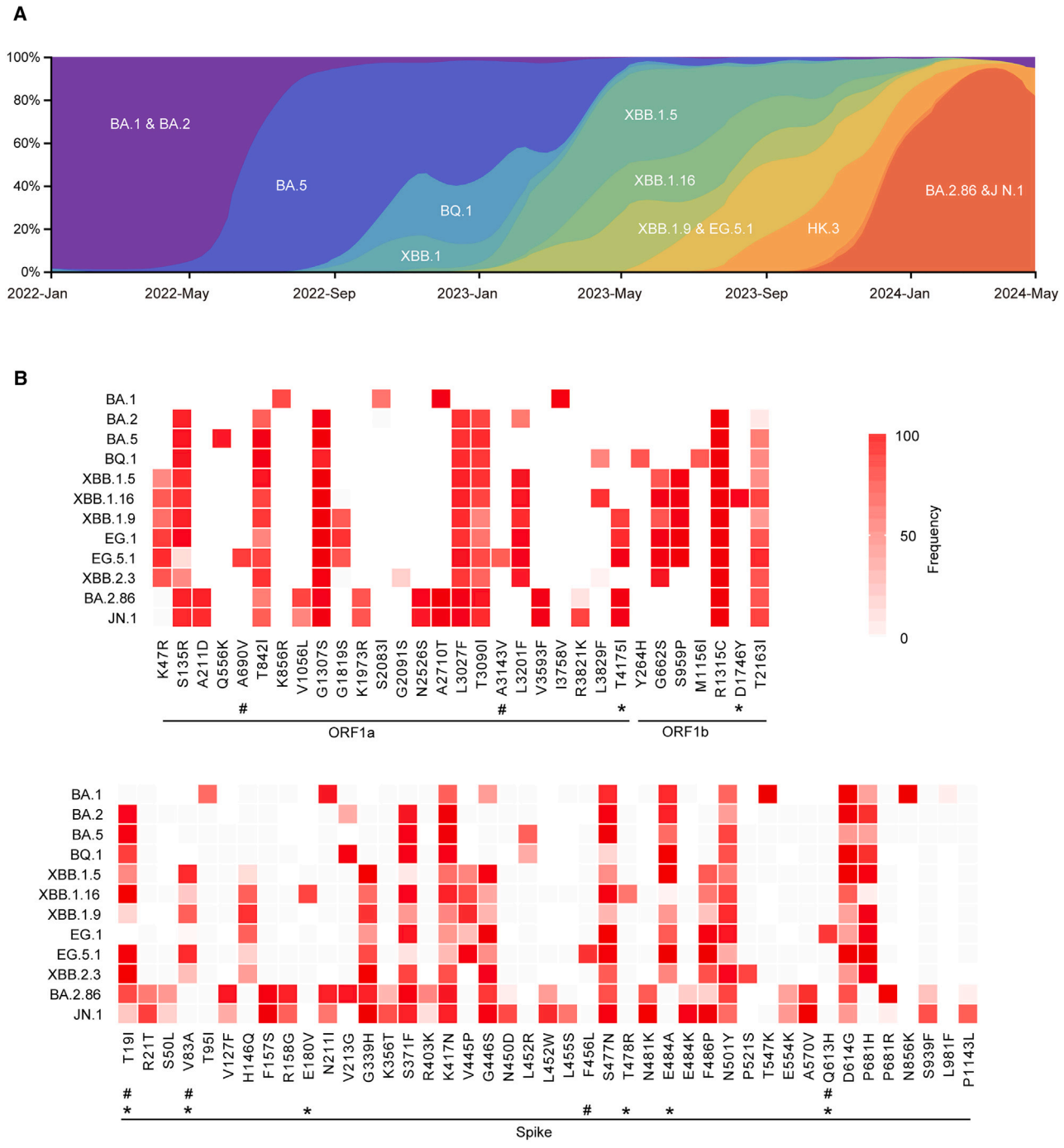

Figure 1. Evolution and mutation patterns of the main variants of SARS-CoV2 Omicron sublineage

(A) Evolution of the prevalence of main SARS-CoV-2 Omicron/XBB sublineages from January 2022 to May 2024. The pattern of the emergence and replacement of several sublineages, such as BA.1/BA.2, BA.5, BQ.1, XBB.1.5, XBB.1.16, XBB.1.9, EG.5.1, HK.3 and BA.2.86/JN.1 is shown.

(B) Frequency of mutations of interest in the representative Omicron/XBB sublineages on the ORF1a/b and Spike genes. The mutations on the genes of ORF3a, E, M, ORF6, ORF7a/b, ORF8, and so forth. Are shown in Figure S1. The different mutations between EG.1 and XBB.1.16 are marked by asterisk. The different mutations between EG.1 and EG.5.1 are marked by "#."

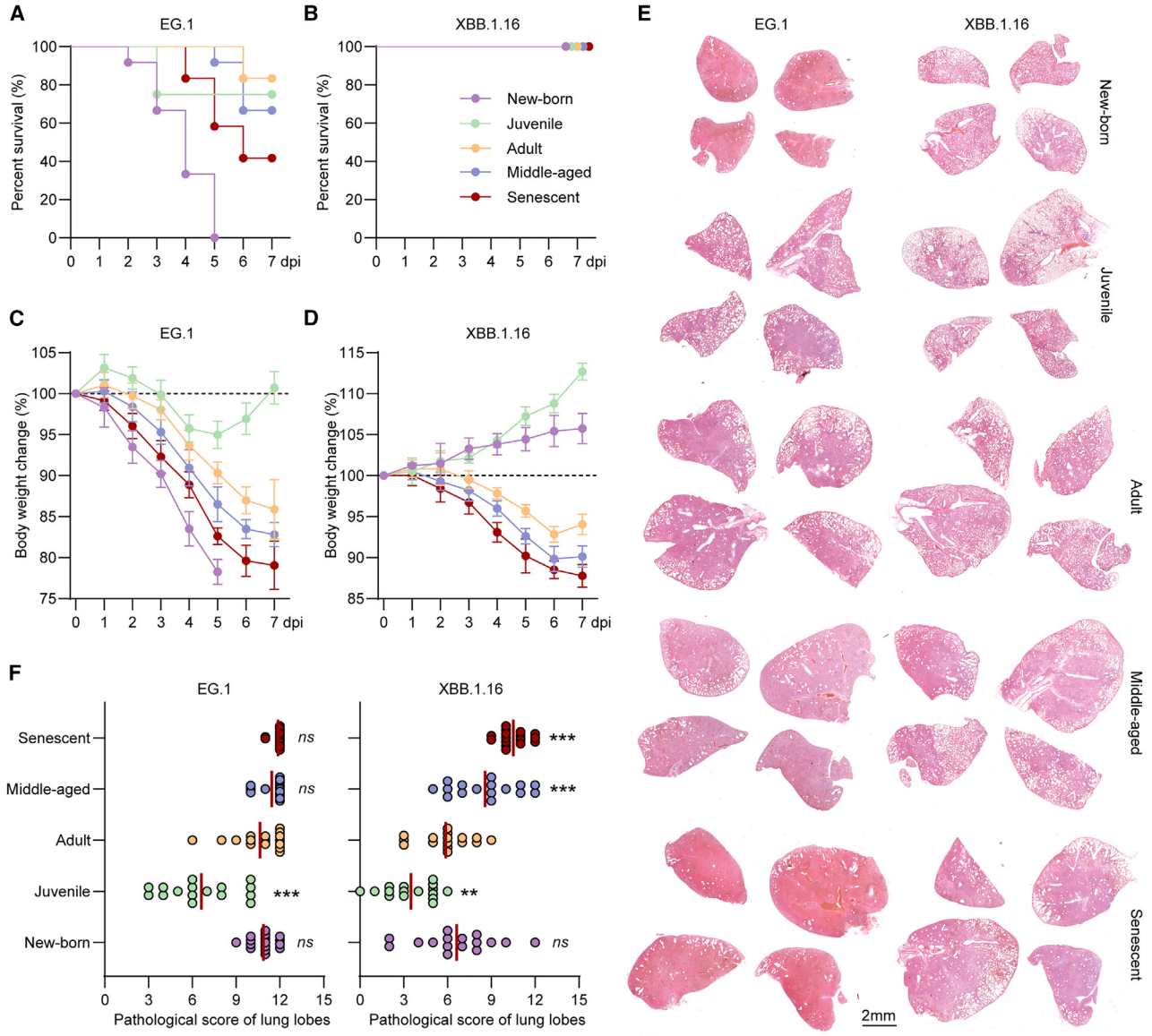

Figure 2. Disease outcome of SARS-CoV-2 EG.1 and XBB.1.16 infections in different age groups of hamsters

The new-born, juvenile, adult, middle-aged and senescent hamsters were infected with 1 × 10^5 PFU of EG.1 or XBB.1.16 by nasal route, respectively.

(A and B) Survival rates were recorded from 0 to 7 dpi (n = 12/group).

(C and D) Body weight changes of the survived hamsters were detected (n = 4/group).

(E) Representative images for H&E staining of lung lobes collected from the deceased new-born hamsters (5 dpi) and the euthanized juvenile, adult, middle-aged and senescent hamsters (7 dpi) were shown (bar = 2 mm). Images for all of the lung tissues collected from each age group were shown in Figure S2 and S3.

(F) Comprehensive pathological scores for lung lobes were determined based on the severity and percentage of injured areas of each lung lobe. For each group, approximately 16 lung lobes were collected from four individual hamsters and were scored (Table. S1). Data are represented as mean ± SD. Significance was determined by one-way ANOVA. Two-sided p-values <0.01 were considered significant: *p < 0.01, **p < 0.001, ***p < 0.0001, ns indicates no significance.

solid organs, including the heart, liver, spleen and kidney by real-time reverse transcription polymerase chain reaction (RT-PCR) that amplifies SARS-CoV-2 open reading frame 1ab (ORF1ab) for the detection of viral RNA levels in these homogenized tissues. After the infection of EG.1, the new-born, juvenile, adult, middle-aged and senescent hamsters showed viral RNA levels of 9.01 ± 0.37, 8.03 ± 0.48, 7.74 ± 0.34, 8.35 ± 0.42 and 8.83 ± 0.35 $\log_{10}$ (copies/mL) in nasal turbinate (Figure 3A, top); 8.42 ± 0.49, 7.72 ± 0.35, 7.17 ± 0.30, 8.07 ± 0.46 and 8.12 ± 0.41 $\log_{10}$ (copies/mL) in trachea (Figure 3B, top); 8.94 ± 0.27, 7.98 ± 0.49, 7.61 ± 0.32, 8.51 ± 0.31 and 8.75 ± 0.40 $\log_{10}$ (copies/mL) in lung (Figure 3C, top); 7.40 ± 0.35, 6.12 ± 0.30, 5.68 ± 0.44, 6.39 ± 0.43 and 6.50 ± 0.31 $\log_{10}$ (copies/mL) in heart (Figure 3D, top); 7.08 ± 0.46, 5.81 ± 0.33, 5.47 ± 0.46, 5.95 ± 0.55 and 5.90 ± 0.37 $\log_{10}$ (copies/mL) in liver (Figure 3E, top); 6.91 ± 0.37, 5.81 ± 0.35, 4.96 ± 0.33, 5.51 ± 0.27 and 5.95 ± 0.47 $\log_{10}$

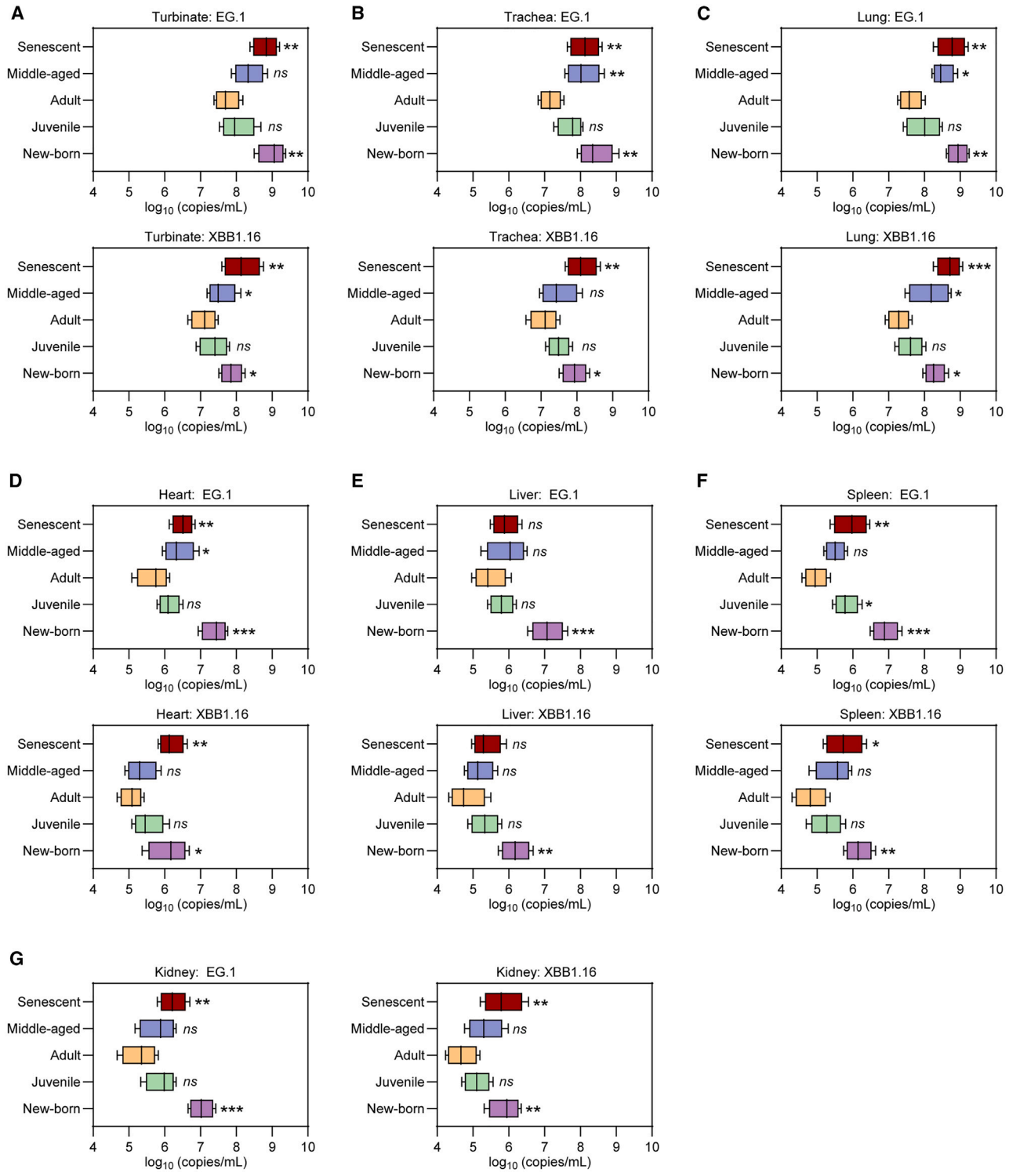

Figure 3. Viral load in multiple organs of the hamsters infected with SARS-CoV-2 EG.1 and XBB.1.16 infections

Viral RNA levels in (A) nasal turbinate, (B) trachea, (C) lung, (D) heart, (E) liver, (F) spleen and (G) kidney that collected from the new-born, juvenile, adult, middle-aged and senescent hamsters euthanized at 7 dpi were measured by RT-PCR, respectively (n = 4/group). In particular, the tissue samples of the EG.1-infeced new-born hamsters were collected from those diseased at 5 dpi. Primers targeting the SARS-CoV-2 ORF1ab gene were used for amplification. Data are represented as mean ± SD. Significance was determined by one-way ANOVA. Two-sided p-values <0.01 were considered significant: $^{*}p < 0.01$, $^{**}p < 0.001$, $^{***}p < 0.0001$, ns indicates no significance.

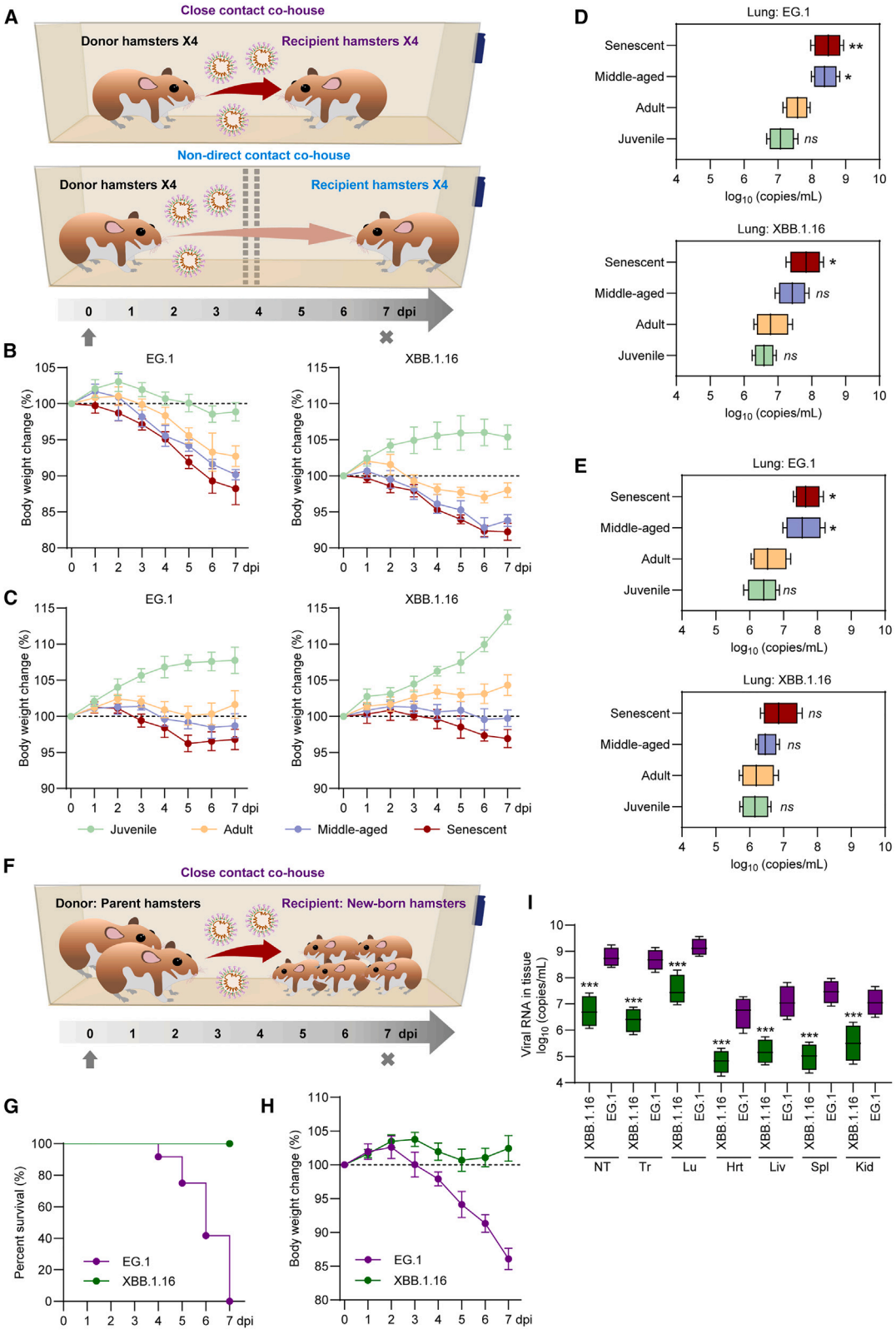

(legend on next page)

(copies/mL) in spleen (Figure 3F, top); 7.03 ± 0.33, 5.91 ± 0.42, 5.30 ± 0.48, 5.82 ± 0.50 and 6.23 ± 0.37 log_{10} (copies/mL) in kidney (Figure 3G, left), respectively. After the infection of XBB.1.16, the new-born, juvenile, adult, middle-aged and senescent hamsters showed viral RNA levels of 7.86 ± 0.30, 7.37 ± 0.41, 7.09 ± 0.35, 7.57 ± 0.40 and 8.51 ± 0.51 log_{10} (copies/mL) in nasal turbinate (Figure 3A, bottom); 7.93 ± 0.35, 7.50 ± 0.31, 7.08 ± 0.39, 7.49 ± 0.51 and 8.14 ± 0.42 log_{10} (copies/mL) in trachea (Figure 3B, bottom); 8.29 ± 0.30, 7.61 ± 0.36, 7.28 ± 0.31, 8.15 ± 0.58 and 8.69 ± 0.34 log_{10} (copies/mL) in lung (Figure 3C, bottom); 6.10 ± 0.55, 5.53 ± 0.44, 5.07 ± 0.32, 5.35 ± 0.42 and 6.18 ± 0.36 log_{10} (copies/mL) in heart (Figure 3D, bottom); 6.19 ± 0.40, 5.33 ± 0.38, 4.83 ± 0.50, 5.18 ± 0.39 and 5.37 ± 0.41 log_{10} (copies/mL) in liver (Figure 3E, bottom); 6.17 ± 0.37, 5.26 ± 0.45, 4.82 ± 0.44, 5.47 ± 0.50 and 5.76 ± 0.52 log_{10} (copies/mL) in spleen (Figure 3F, bottom); 5.89 ± 0.43, 5.11 ± 0.36, 4.69 ± 0.41, 5.34 ± 0.50 and 5.83 ± 0.55 log_{10} (copies/mL) in kidney, respectively (Figure 3G, right). After infection with both EG.1 and XBB.1.16, the new-born and senescent hamsters showed higher levels of viral RNA in all organs than those in other age groups. In all age groups and organs, EG.1 showed similar and/or higher levels of viral RNA than XBB.1.16, suggesting a more robust viral replication (Figure S4). In our previous studies, infectious viral particle was rarely detectable in the lung tissues collected at 7 dpi.[10] In this study, because most of the tissue samples were collected at 7 dpi, we only detected the infectious viral particle levels in tissues of the EG.1-infected new-born hamsters diseased at 5 dpi by a TCID50 method. As expected, high levels of infectious viral particle were found in all the detected tissues (Figure S5).

Assessment of the transmissibility of severe acute respiratory syndrome coronavirus 2 EG.1 and XBB.1.16 variants in hamsters of all ages

Furthermore, we evaluated the transmissibility of SARS-CoV-2 EG.1 and XBB.1.16 variants among the juvenile, adult, middle-aged and senescent hamsters by close contact co-house and non-direct contact co-house. Four donor hamsters were inoculated with 1 × 10^5 PFU of EG.1 or XBB.1.16 by nasal route, and then co-housed with four age-paired naive recipient hamsters for seven days (Figure 4A). All of the hamsters survived at 7 dpi. After close contact co-house of EG.1 donor hamsters, the juvenile, adult, middle-aged and senescent recipient hamsters showed 1.1 ± 1.2%, 7.2 ± 1.4%, 9.8 ± 0.7% and 11.8 ± 2.2% of body weight loss from 0 to 7 dpi, respectively (Figure 4B, left). The juvenile recipient hamsters showed 5.4 ± 1.7% of body weight increase after a seven-day close contact co-house of XBB.1.16 donor hamsters (Figure 4B, right). Whereas the adult, middle-aged and senescent recipient hamsters showed 2.0 ± 1.1%, 6.2 ± 0.8% and 7.7 ± 1.2% of body weight loss (Figure 4B, left). After non-direct contact co-house of EG.1 or XBB.1.16 donor hamsters, the juvenile recipient hamsters showed over 5% of body weight increase, the adult recipient hamsters showed slight increase of body weight, the middle-aged and senescent recipient hamsters showed less than 5% of body weight loss from 0 to 7 dpi, respectively (Figure 4C).

We then euthanized the recipient hamsters at 7 dpi for the measurement of viral RNA in lung tissues. For the course of close contact co-house of EG.1, the juvenile, adult, middle-aged and senescent recipient hamsters showed viral RNA levels of 7.10 ± 0.38, 7.57 ± 0.33, 8.39 ± 0.35 and 8.47 ± 0.41 log_{10} (copies/mL) in lung (Figure 4D, top); those close contacted with XBB.1.16 donor hamsters showed viral RNA levels of 6.59 ± 0.29, 6.82 ± 0.48, 7.42 ± 0.41 and 7.82 ± 0.46 log_{10} (copies/mL) in lung, respectively (Figure 4D, bottom). For the course of non-direct contact co-house of EG.1, the juvenile, adult, middle-aged and senescent recipient hamsters showed viral RNA levels of 6.38 ± 0.44, 6.58 ± 0.50, 7.58 ± 0.52 and 7.69 ± 0.37 log_{10} (copies/mL) in lung (Figure 4E, top); those co-housed with XBB.1.16 donor hamsters showed showed viral RNA levels of 6.16 ± 0.39, 6.23 ± 0.49, 6.50 ± 0.30 and 6.91 ± 0.51 log_{10} (copies/mL) in lung, respectively (Figure 4E, bottom). Taken together, EG.1 and XBB.1.16 showed 100% transmission rate among the juvenile, adult, middle-aged and senescent hamsters by the routes of both close contact co-house and non-direct contact co-house. Close contact co-housing infection resulted in a worse severe disease outcome than non-direct contact co-housing infection.

To evaluate the transmissibility of new-born hamsters, the parent hamsters were inoculated with 1 × 10^5 PFU of EG.1 or XBB.1.16 by nasal route as donor hamsters, and then close contacted with the naive new-born hamsters for seven days (Figure 4F). All of the new-born hamsters deceased within seven days contact with EG.1 donors (Figure 4G). Whereas, those contacted with XBB.1.16 donor hamsters survived (Figure 4G). The new-born hamsters contacted with EG.1 donors showed nearly 15% of body weight loss and those contacted with XBB.1.16 donors showed slight body weight increase at 7 dpi (Figure 4H).

Figure 4. Assessment of the transmissibility of SARS-CoV-2 EG.1 and XBB.1.16 variants in hamsters of all ages

(A) Graphic illustration for close contact co-house and non-direct contact co-house. For the juvenile, adult, middle-aged and senescent hamsters, four donors were infected with 1 × 10^5 PFU of EG.1 or XBB.1.16 by nasal route, and co-housed with four age-paired naive recipients for seven days. In the situation of close contact co-house, the donors and the recipients can have full intimate contact in the isolation cage. In the situation of non-direct contact co-house, the donors and the recipients were separated by double-layer grid. Body weight changes of recipient hamsters from 0 to 7 dpi of (B) close contact co-house and (C) non-direct contact co-house were recorded (n = 4/group). Viral RNA levels in lungs that collected from the juvenile, adult, middle-aged and senescent hamsters euthanized at 7 dpi of (D) close contact co-house and (E) non-direct contact co-house were measured by RT-PCR, respectively (n = 4/group). (F) Graphic illustration for close contact co-house of new-born hamsters. Both of the parent hamsters were infected with 1 × 10^5 PFU of EG.1 or XBB.1.16 by nasal route, and co-housed with the naive recipient new-born hamsters for seven days.

(G) Survival rates of the recipient new-born hamsters were recorded from 0 to 7 dpi (n = 12/group).

(H) Body weight changes of the survived hamsters were detected (n = 4/group). Viral RNA levels in nasal turbinate (NT), trachea (Tr), lung (Lu), heart (Hrt), liver (Liv), spleen (Spl) and kidney (Kid) that collected from the recipient new-born hamsters deceased (EG.1) or euthanized (XBB.1.16) at 7 dpi were measured by RT-PCR, respectively (n = 4/group). Data are represented as mean ± SD. Significance was determined by one-way ANOVA. Two-sided p-values <0.01 were considered significant: *p < 0.01, **p < 0.001, ***p < 0.0001, ns indicates no significance.

Furthermore, the new-born hamsters contacted with EG.1 donors showed significant higher viral RNA levels in respiratory tract organs including nasal turbinate, trachea and lung, as well as the main solid organs include heart, liver, spleen and kidney than those contacted with XBB.1.16 donors at 7 dpi (Figure 4H). These data suggested that EG.1 and XBB.1.16 are 100% transmissible from the parent hamsters to the new-born hamsters by the route of both close contact co-house. Of note, EG.1 showed a higher transmissibility than XBB.1.16 in all age groups of hamsters.

DISCUSSION

Although the SARS-CoV-2 pandemic has ended, local epidemics of emerging variants are still causing significant disease burden. Therefore, the study of viral surveillance and changes in the pathogenicity and transmissibility of different variants remains a long-term task to improve our basic understanding of SARS-CoV-2 evolution. The Syrian hamster model has been shown to be sensitive to SARS-CoV-2 infection, transmission and pathology, and provides a stable platform for *in vivo* studies of SARS-CoV-2 variants.[11–14] Early SARS-CoV-2 variants (Alpha, Beta, Gamma and Delta) usually cause high mortality in adult hamsters from 5 to 7 dpi, with 15%–30% of body loss at the endpoints (7 dpi).[14,15] After the significant attenuation of pathogenicity in Omicron BA.1 [9,10] the vast majority of the following SARS-CoV-2 variants such as BA.2, BA.4, BA.5, BQ.1, and XBB usually causes mild to moderate illness in both human patients, as well as reduced mortality, body weight loss, and lung injury in animal models than those infected with prototype or Delta variant.[5–7,9,16,17] Several viral and host factors might affect the disease outcomes of SARS-CoV-2 infection.[18] For instance, high exposure viral load lead to higher mortality, body weight loss, and lung injury than those inoculated with lower viral load, especially in the aged hamsters.[19]

Here, we present a specific SARS-CoV-2 EG.1 variant with significantly enhanced pathogenicity and transmissibility in the hamster model. The high mortality, rapid body weight loss and severe lung injury of EG.1-infected hamsters revealed that a few XBB variants could evolve to be highly pathogenic. Meanwhile, the relatively mild XBB.1.16 variant showed more severe symptoms in new-born, middle-aged, and senescent hamsters than in adult hamsters. Similar to previous studies of earlier SARS-CoV-2 variants, these data confirmed the age-dependent disease outcome of XBB variant infections. On the other hand, we also detected viral RNA levels in non-respiratory organs, including heart, liver, spleen and kidney. For both EG.1 and XBB.1.16, viral loads in these organs showed an age-dependent pattern, indicating a risk of multi-organ failure and sequelae. The Q613H mutation in EG.1 was first reported in the Alpha variant (A.23)[20] and also detected in the Delta variant (AY.33) and relevant sublineages.[21,22] Similar to the well-known D614G mutation, Q613H mutation is likely to cause increased pathogenicity and transmissibility by enhancing the bind between SARS-CoV-2 spike and receptor protein ACE2.[21] In addition, the reversion of Q613H in A.23.1 variant of SARS-CoV-2 resulted in 9.5-fold decrease of infectivity than the ancestral residue.[23] Together with our sequence analysis results, we speculate that Q613H mutation might be contribute to the increased pathogenicity and transmissibility of EG.1 variant. Fortunately, the epidemic of EG.1 and its relevant variants, such as XBB.1.9 and EG.5.1, lasted only a few months in 2023 and was replaced by new variants with relatively low pathogenicity, such as BA.2.86 and JN.1. However, as the virus evolves over time and the trend is unexpected, there is still a risk of new highly pathogenic SARS-CoV-2 variants emerging in the foreseeable future, which requires continuous monitoring of circulating variants of interest.

Limitations of the study

The sex dimorphism of SARS-CoV-2 infection and disease outcome has been well documented in previous studies. In general, males tend to develop more severe symptoms than females.[24–29] To avoid the potential effects of sex dimorphism, we used only male juvenile, adult, middle-aged and senescent hamsters in this study. Due to the time constraints of the BSL-3 laboratory, we did not investigate the relationship between the specific mutations on EG.1 and its unique virological properties.

RESOURCE AVAILABILITY

Lead contact

Further information and requests for resources and reagents should be directed to and will be fulfilled by Dr. Lunzhi Yuan (yuanlunzhi@xmu.edu.cn).

Materials availability

All unique/stable reagents generated in this study are available from the lead contact with a completed materials transfer agreement.

Data code and availability

- All data reported in this article will be shared by the lead contact upon request.
- This article does not report the original code.
- In this study, we used the genomic sequences of the SARS-CoV-2 variant deposited in the public EpiCoV databse of Global Initiative on Sharing All Influenza Data (GISAID) (http://www.gisaid.org).

ACKNOWLEDGMENTS

This work was supported by grants from the National Science Key Research and Development Project (2022YFC0870800), National Natural Science Foundation of China (82272305), Hong Kong Research Grant Council (T11-705/21-N and T11-712/19-N) and the Innovation and Technology Commission of Hong Kong (with funding support to SKLEID).

AUTHOR CONTRIBUTIONS

Z,M., M.J., F.M.J., and L.X. contributed equally to this work. Z.M., M.J., Z.H.C., and C.P.W. prepared the virus stocks and analyzed viral sequences. Y.L.Z., Z.M., W.K., Y.J.H., C.P.W., and C.R.R. performed animal experiments and sample measurements. F.M.J., X.L., C.Z., Z.Y.L., and Y.Q. participated in project design and provided proposals. Y.L.Z., Z.M., and L.X. wrote the article. Z.H.C., G.Y., X.N.S., C.T., and Y.L.Z. supervised this study.

DECLARATION OF INTERESTS

The authors declare no competing interests.

STAR★METHODS

Detailed methods are provided in the online version of this paper and include the following:

- KEY RESOURCES TABLE
- EXPERIMENTAL MODEL AND SUBJECT DETAILS
  - Phylogenetic tree inference and lineage monitoring
  - Experimental animal and biosafety
  - Virus stock
- METHOD DETAILS
  - Virus inoculation and sample collection
  - Detection of viral RNA and titers of infectious viral particles
  - Pathological studies
- QUANTIFICATION AND STATISTICAL ANALYSIS
  - Animal and sample size justification
  - Statistical analysis

SUPPLEMENTAL INFORMATION

Supplemental information can be found online at https://doi.org/10.1016/j.isci.2025.111875.

Received: June 6, 2024
Revised: November 16, 2024
Accepted: January 20, 2025
Published: January 22, 2025

REFERENCES

1. Halfmann, P.J., Iida, S., Iwatsuki-Horimoto, K., Maemura, T., Kiso, M., Scheaffer, S.M., Darling, T.L., Joshi, A., Loeber, S., Singh, G., et al. (2022). SARS-CoV-2 Omicron virus causes attenuated disease in mice and hamsters. Nature *603*, 687–692. https://doi.org/10.1038/s41586-022-04441-6.
2. Shuai, H., Chan, J.F.W., Hu, B., Chai, Y., Yuen, T.T.T., Yin, F., Huang, X., Yoon, C., Hu, J.C., Liu, H., et al. (2022). Attenuated replication and pathogenicity of SARS-CoV-2 B.1.1.529 Omicron. Nature *603*, 693–699. https://doi.org/10.1038/s41586-022-04442-5.
3. Suzuki, R., Yamasoba, D., Kimura, I., Wang, L., Kishimoto, M., Ito, J., Morioka, Y., Nao, N., Nasser, H., Uriu, K., et al. (2022). Attenuated fusogenicity and pathogenicity of SARS-CoV-2 Omicron variant. Nature *603*, 700–705. https://doi.org/10.1038/s41586-022-04462-1.
4. Uraki, R., Kiso, M., Iida, S., Imai, M., Takashita, E., Kuroda, M., Halfmann, P.J., Loeber, S., Maemura, T., Yamayoshi, S., et al. (2022). Characterization and antiviral susceptibility of SARS-CoV-2 Omicron BA.2. Nature *607*, 119–127. https://doi.org/10.1038/s41586-022-04856-1.
5. Uraki, R., Halfmann, P.J., Iida, S., Yamayoshi, S., Furusawa, Y., Kiso, M., Ito, M., Iwatsuki-Horimoto, K., Mine, S., Kuroda, M., et al. (2022). Characterization of SARS-CoV-2 Omicron BA.4 and BA.5 isolates in rodents. Nature *612*, 540–545. https://doi.org/10.1038/s41586-022-05482-7.
6. Ito, J., Suzuki, R., Uriu, K., Itakura, Y., Zahradnik, J., Kimura, K.T., Deguchi, S., Wang, L., Lytras, S., Tamura, T., et al. (2023). Convergent evolution of SARS-CoV-2 Omicron subvariants leading to the emergence of BQ.1.1 variant. Nat. Commun. *14*, 2671. https://doi.org/10.1038/S41467-023-38188-Z.
7. Tamura, T., Ito, J., Uriu, K., Zahradnik, J., Kida, I., Anraku, Y., Nasser, H., Shofa, M., Oda, Y., Lytras, S., et al. (2023). Virological characteristics of the SARS-CoV-2 XBB variant derived from recombination of two Omicron subvariants. Nat. Commun. *14*, 2800. https://doi.org/10.1038/S41467-023-38435-3.
8. Yuan, L., Zhu, H., Chen, P., Zhou, M., Ma, J., Liu, X., Wu, K., Chen, R., Liu, Q., Yu, H., et al. (2022). Infection, pathology and interferon treatment of the SARS-CoV-2 Omicron BA.1 variant in juvenile, adult and aged Syrian hamsters. Cell. Mol. Immunol. *19*, 1392–1399. https://doi.org/10.1038/s41423-022-00923-9.
9. Tamura, T., Irie, T., Deguchi, S., Yajima, H., Tsuda, M., Nasser, H., Mizuma, K., Plianchaisuk, A., Suzuki, S., Uriu, K., et al. (2024). Virological characteristics of the SARS-CoV-2 Omicron XBB.1.5 variant. Nat. Commun. *15*, 1176. https://doi.org/10.1038/S41467-024-45274-3.
10. Yuan, L., Zhu, H., Zhou, M., Ma, J., Chen, R., Yu, L., Chen, W., Hong, W., Wang, J., Chen, Y., et al. (2022). Persisting lung pathogenesis and minimum residual virus in hamster after acute COVID-19. Protein Cell *13*, 72–77. https://doi.org/10.1007/s13238-021-00874-3.
11. Yuan, L., Zhu, H., Zhou, M., Ma, J., Liu, X., Wu, K., Ye, J., Yu, H., Chen, P., Chen, R., et al. (2022). Nasal irrigation efficiently attenuates SARS-CoV-2 Omicron infection, transmission and lung injury in the Syrian hamster model. iScience *25*, 105475. https://doi.org/10.1016/j.isci.2022.105475.
12. Imai, M., Iwatsuki-Horimoto, K., Hatta, M., Loeber, S., Halfmann, P.J., Nakajima, N., Watanabe, T., Ujie, M., Takahashi, K., Ito, M., et al. (2020). Syrian hamsters as a small animal model for SARS-CoV-2 infection and countermeasure development. Proc. Natl. Acad. Sci. USA *117*, 16587–16595. https://doi.org/10.1073/pnas.2009799117.
13. Chan, J.F.W., Zhang, A.J., Yuan, S., Poon, V.K.M., Chan, C.C.S., Lee, A.C.Y., Chan, W.M., Fan, Z., Tsoi, H.W., Wen, L., et al. (2020). Simulation of the Clinical and Pathological Manifestations of Coronavirus Disease 2019 (COVID-19) in a Golden Syrian Hamster Model: Implications for Disease Pathogenesis and Transmissibility. Clin. Infect. Dis. *71*, 2428–2446. https://doi.org/10.1093/cid/ciaa325.
14. Abdelnabi, R., Boudewijns, R., Foo, C.S., Seldeslachts, L., Sanchez-Felipe, L., Zhang, X., Delang, L., Maes, P., Kaptein, S.J.F., Weynand, B., et al. (2021). Comparing infectivity and virulence of emerging SARS-CoV-2 variants in Syrian hamsters. EBioMedicine *68*, 103403. https://doi.org/10.1016/j.ebiom.2021.103403.
15. Rosenke, K., Meade-White, K., Letko, M., Clancy, C., Hansen, F., Liu, Y., Okumura, A., Tang-Huau, T.L., Li, R., Saturday, G., et al. (2020). Defining the Syrian hamster as a highly susceptible preclinical model for SARS-CoV-2 infection. Emerg. Microb. Infect. *9*, 2673–2684. https://doi.org/10.1080/22221751.2020.1858177.
16. Halfmann, P.J., Iwatsuki-Horimoto, K., Kuroda, M., Hirata, Y., Yamayoshi, S., Iida, S., Uraki, R., Ito, M., Ueki, H., Furusawa, Y., et al. (2024). Characterization of Omicron BA.4.6, XBB, and BQ.1.1 subvariants in hamsters. Commun. Biol. *7*, 331. https://doi.org/10.1038/s42003-024-06015-w.
17. Tamura, T., Yamasoba, D., Oda, Y., Ito, J., Kamasaki, T., Nao, N., Hashimoto, R., Fujioka, Y., Suzuki, R., Wang, L., et al. (2023). Comparative pathogenicity of SARS-CoV-2 Omicron subvariants including BA.1, BA.2, and BA.5. Commun. Biol. *6*, 772. https://doi.org/10.1038/s42003-023-05081-w.
18. Griffin, B.D., Warner, B.M., Chan, M., Valcourt, E., Tailor, N., Banadyga, L., Leung, A., He, S., Boese, A.S., Audet, J., et al. (2021). Host parameters and mode of infection influence outcome in SARS-CoV-2-infected hamsters. iScience *24*, 103530. https://doi.org/10.1016/J.Isci.2021.103530.
19. Xuan, L., Ming, Z., Fang, M., Xie, Y., Chen, P., Chen, R., Wu, K., Ye, J., Liu, C., Zhu, H., et al. (2024). Decisive reversal of lethal coronavirus disease 2019 in senescent hamster by synchronic antiviral and immunoregulatory intervention. Med. Comm. *5*, e642. https://doi.org/10.1002/mco2.642.
20. Bugembe, D.L., Phan, M.V.T., Ssewanyana, I., Semanda, P., Nansumba, H., Dhaala, B., Nabadda, S., O'Toole, Á.N., Rambaut, A., Kaleebu, P., and Cotten, M. (2021). Emergence and spread of a SARS-CoV-2 lineage A variant (A.23.1) with altered spike protein in Uganda. Nat. Microbiol. *6*, 1094–1101. https://doi.org/10.1038/s41564-021-00933-9.
21. Peacock, T.P., Penrice-Randal, R., Hiscox, J.A., and Barclay, W.S. (2021). SARS-CoV-2 one year on: evidence for ongoing viral adaptation. J. Gen. Virol. *102*, 001584. https://doi.org/10.1099/Jgv.0.001584.
22. Mannsverk, S., Bergholm, J., Palanisamy, N., Ellström, P., Kaden, R., Lindh, J., and Lennerstrand, J. (2022). SARS-CoV-2 variants of concern and spike protein mutational dynamics in a Swedish cohort during 2021,

studied by Nanopore sequencing. Virol. J. *19*, 164. https://doi.org/10.1186/s12985-022-01896-x.

23. Yurkovetskiy, L., Shawn, E., Kurhade, C., Diaz-Salinas, M.A., Jaimes, J.A., Nyalile, T., Xie, X., Choudhary, M.C., Dauphin, A., Li, J.Z., et al. (2023). S:D614G and S:H655Y are gateway mutations that act epistatically to promote SARS-CoV-2 variant fitness. Preprint at bioRxiv. https://doi.org/10.1101/2023.03.30.535005.
24. Yuan, L., Zhu, H., Zhou, M., Ma, J., Chen, R., Chen, Y., Chen, L., Wu, K., Cai, M., Hong, J., et al. (2021). Gender associates with both susceptibility to infection and pathogenesis of SARS-CoV-2 in Syrian hamster. Signal Transduct. Targeted Ther. *6*, 136. https://doi.org/10.1038/s41392-021-00552-0.
25. Yuan, L., Zhu, H., Wu, K., Zhou, M., Ma, J., Chen, R., Tang, Q., Cheng, T., Guan, Y., and Xia, N. (2022). Female sex hormone, progesterone, ameliorates the severity of SARS-CoV-2-caused pneumonia in the Syrian hamster model. Signal Transduct. Targeted Ther. *7*, 47. https://doi.org/10.1038/s41392-021-00860-5.
26. Peckham, H., de Gruijter, N.M., Raine, C., Radziszewska, A., Ciurtin, C., Wedderburn, L.R., Rosser, E.C., Webb, K., and Deakin, C.T. (2020). Male sex identified by global COVID-19 meta-analysis as a risk factor for death and ITU admission. Nat. Commun. *11*, 6317. https://doi.org/10.1038/s41467-020-19741-6.
27. Meng, Y., Wu, P., Lu, W., Liu, K., Ma, K., Huang, L., Cai, J., Zhang, H., Qin, Y., Sun, H., et al. (2020). Sex-specific clinical characteristics and prognosis of coronavirus disease-19 infection in Wuhan, China: A retrospective study of 168 severe patients. PLoS Pathog. *16*, e1008520. https://doi.org/10.1371/journal.ppat.1008520.
28. Takahashi, T., Ellingson, M.K., Wong, P., Israelow, B., Lucas, C., Klein, J., Silva, J., Mao, T., Oh, J.E., Tokuyama, M., et al. (2020). Sex differences in immune responses that underlie COVID-19 disease outcomes. Nature *588*, 315–320. https://doi.org/10.1038/s41586-020-2700-3.
29. Park, M.D. (2020). Sex differences in immune responses in COVID-19. Nat. Rev. Immunol. *20*, 461. https://doi.org/10.1038/s41577-020-0378-2.

STAR★METHODS

KEY RESOURCES TABLE

REAGENT or RESOURCE	SOURCE	IDENTIFIER
Virus Sequence		
BA.1	GISAID	EPI_ISL_8182026
BA.2		EPI_ISL_10654979
BA.5		EPI_ISL_12920651
BQ.1		EPI_ISL_18983075
XBB.1.5		EPI_ISL_19000756
XBB.1.16		EPI_ISL_17684413
XBB.1.9.1		EPI_ISL_17419152
XBB.1.9.2.1 (EG.1)		EPI_ISL_17660518
EG.5.1		EPI_ISL_17949406
XBB.2.3		EPI_ISL_18991864
XBB.2.86		EPI_ISL_18221650
JN.1		EPI_ISL_18363371
Reagents		
Dulbecco's Modified Eagle Medium (DMEM)	GIBCO	#11995
Fetal bovine serum (FBS)		#10270106
Phosphate buffer saline (PBS)		#10010031
TPCK-trypsin	SIGMA-ALDRICH	#T1426
DMSO		#D5879
Penicillin-Streptomycin	Invitrogen	#15140-122
$MgCl_2$	Thermo Fisher	#AM9530G
Isoflurane	RWD Life Science	#R510-22
Fast-King Strand cDNA Synthesis Kit	TIANGEN	#FP313
QIAamp Viral RNA Mini kit	Qiagen	#52906
SARS-CoV-2 RT-PCR Kit	Wantai	N/A
Hematoxylin	Maxim Biotechnology	#CTS-1096
Eosin		#CTS-4094
Slide		#SLI-20010312

EXPERIMENTAL MODEL AND SUBJECT DETAILS

Phylogenetic tree inference and lineage monitoring

The evolution of the prevalence of SARS-CoV-2 lineages throughout 2024 was visualized using GNU Affero General Public License 3.0 in next strain. This phylogenetic tree was developed with the next strain server by using the date from GISAID between Jun 2020 and Apr 2024. All SARS-CoV-2 sequences are received via direct provision from the GISAID Epicov database (https://gisaid.org/). Mutations that are common and specific to lineages of interest were computed using the date using GISAID data until April 20, 2024, Values for mutations were manually computed.

Experimental animal and biosafety

The Syrian Hamster (LVG strain) was raised in the specific pathogen free animal feeding facilities. All the animal experiments were approved by the Medical Ethics Committee (SUMC2022-051). All experiments with infectious SARS-CoV-2 were performed in the biosafety level 3 (BSL-3) and animal biosafety level 3 (ABSL-3) facilities. Our staff wore powered air-purifying respirators that filtered the air, and disposable coveralls when they cultured the virus and handled animals that were in isolators. The researchers were disinfected before they left the room and then showered on exiting the facility. All facilities, procedures, training records, safety drills, and inventory records were subject to periodic inspections and ongoing oversight by the institutional biosafety officers who consult frequently with the facility managers.

Virus stock

The EG.1 (share an identical sequence with EPI_ISL_17660518) and XBB.1.16 (share an identical sequence with EPI_ISL_17684413) variants were passaged on Vero cells (#CCL-81, ATCC). Viral stocks were prepared in Vero cells with DMEM containing 2% FBS, 5 μg/mL TPCK-trypsin, 1% Penicillin-Streptomycin and 30 mmol/L $MgCl_2$. Viruses were harvested and stored in ultra-low temperature freezer. The titers were determined by means of plaque assay in Vero cells.

METHOD DETAILS

Virus inoculation and sample collection

Hamsters were anesthetized by isoflurane (#R510-22, RWD Life Science) and nasally inoculated with indicated doses of SARS-CoV-2 diluted in PBS (#10010031, GIBCO). The new-born (male and female, ∼1 week), juvenile (male, 4–5 weeks), adult (male, 10–12 weeks), middle-aged (male, ∼40 weeks) and senescent (male, ∼80 weeks) hamsters were inoculated with 1×10^5 PFU of EG.1 or XBB.1.16 by nasal route, respectively. The new-born hamsters received an inoculation volume of 50 μL and the other age group received an inoculation volume of 200 μL. In the infection course, body weight of these hamsters were measured by an electronic balance. Hamsters were euthanized at the indicated time point for detection of viral load in respiratory tract organs and pathological examination in lung lobes.

Detection of viral RNA and titers of infectious viral particles

For the solid organ samples, we collect 1mg turbinate, 0.1 mg trachea and 0.1 mg lung in 1mL PBS for homogenate and detection of viral RNA and viral titer. Viral RNA was extracted by using a QIAamp Viral RNA Mini kit (#52906, Qiagen) according to the manufacturer's instructions. The RT-PCR was conducted by using the SLAN-96S Real-Time System (Hongshi, Shanghai, China) with a SARS-CoV-2 RT-qPCR Kit from Wantai (Beijing, China). Relative Viral RNA of SARS-CoV-2 ORF1ab gene was determined using primer pairs and probes provided in the kit. Viral RNA copies were expressed on a $\log_{10}$ scale after normalized to the standard curve obtained by using 10-fold dilutions of a SARS-CoV-2 stock. The titers of homogenized tissues were measured by plaque assay and half tissue culture infective dose (TCID50) titration method in Vero cells seeded in 96-well plates. In the TCID50 titration assay, Vero cells were incubated with 100 μL of original tissue homogenates and 10-fold serial diluted samples for 1 h. Then, we renewed fresh medium and observed CPE at 3 days after incubation. We defined that all cells without cytopathic effect indicate ''zero''.

Pathological studies

For pathological analysis, lung tissues were fixed in formalin for more than 72 h, dehydrated and then embedded in paraffin wax. The wax block of lung tissues was cut into 4μm sections for pathological staining and analysis. H&E staining was employed for analysis of general lung pathogenic lesions including pulmonary edema, consolidation and inflammation. The standards for pathological score of lung tissues in this study are derived from our previous study in hamster model. Comprehensive pathological scoring of lung sections was performed according to the degree of lung lesions including alveolar septum hyperplasia, consolidation and impairment of alveolar structure, fluid exudation, mucus suppository, thrombus, inflammation recruitment and infiltration of immune cells in each individual lung lobe. For each hamster, three or four lung lobes were employed for evaluation of comprehensive pathological score. In brief, H&E staining result of each lung lobe was analyzed for its severity of pathological change. The pathological score included: a) Alveolar septum thickening and consolidation; b) Hemorrhage, exudation, pulmonary edema and mucous; c) Recruitment and infiltration of inflammatory immune cells. For each issue, scores were related to the severity: 0 indicated no pathological change was observed, 1 indicated moderate pathological change, 2 indicated mild pathological change, 3 indicated severe pathological change and 4 indicated very severe pathological change. In conclusion, scores of such three issues were added as the comprehensive pathological score of a lung lobe, and the average comprehensive pathological score of the lobes indicated the severity of lung pathology in an evaluated hamster. The pathological reagents include Hematoxylin (#CTS-1096) and Eosin (#CTS-4094) were purchased from Maxim Biotechnology (Fuzhou, China). The images of whole lung lobes were screened by a high-throughput screening microscope system (EVOS M7000, Invitrogen of Thermo Fisher Scientific).

QUANTIFICATION AND STATISTICAL ANALYSIS

Animal and sample size justification

Sample sizes maximized considering limits in BSL-3 working capacity, numbers of animals that can be handled under ABSL-3 conditions and availability of well-trained staffs.

Statistical analysis

Student's unpaired two-tailed t-test, one-way ANOVA and were performed using GraphPad Prism 8.0 (GraphPad Software). Data are presented as the means ± SD. Two-sided *p*-values <0.01 were considered significant: $*p < 0.01$, $**p < 0.001$, $***p < 0.0001$, *ns* indicates no significance.